Low-latitude solar wind during the Fall 1998 SOHO-Ulysses quadrature

G. Poletto,[1] S. T. Suess,[2] D. A. Biesecker,[3] R. Esser,[4] G. Gloeckler,[5] Y.-K. Ko,[4] and T. H. Zurbuchen[6]

Received 24 August 2001; revised 29 October 2001; accepted 6 November 2001; published 16 October 2002.

[1] The Fall 1998 Solar and Heliospheric Observatory (SOHO)-Ulysses quadrature occurred when Ulysses was at 5.2 AU, 17.4°S of the equator, and off the west limb of the Sun. SOHO coronal observations, at heliocentric distances of a few solar radii, showed that the line through the solar center and Ulysses crossed, over the first days of observations, a dark, weakly emitting area and through the northern edge of a streamer complex during the second half of the quadrature campaign. Ulysses in situ observations showed this transition to correspond to a decrease from higher-speed wind typical of coronal hole flow to low-speed wind. Physical parameters of the low-latitude coronal plasma sampled over the campaign are determined using constraints from what is the same plasma measured later in situ and simulating the intensities of the hydrogen Lyman-α and OVI 1032 and 1037 Å lines, measured by the Ultraviolet Coronagraph Spectrometer on SOHO. It appears that low-latitude wind from small coronal holes and polar wind have different characteristics in the corona, differences well known at interplanetary distances through in situ experiments. Small, low-latitude coronal holes have a higher expansion factor than typical polar holes, and their plasma moves at a lower speed than plasma from polar holes, reaching, at 3.5 R_{sun}, only about one-fifth of the terminal speed. Wind emanating from bright regions, above streamer complexes, is, at the altitudes we analyzed (i.e., 3.5 and 4.5 R_{sun}), about a factor 3 slower than the low-latitude coronal hole wind, implying a shift to even higher altitudes of the region where plasma gets accelerated. We surmise that open field regions, interspersed amidst closed coronal loops/streamers, may be at least partially responsible for the well-known slow wind speed variability. As in polar fast wind, OVI ions move faster than protons, over the range of altitudes we sampled, and are frozen-in at temperatures of $\approx 1.3-1.5\ 10^6$ K, depending on the site where the outflow originates. An oxygen abundance variation from a value of 8.55, in low-latitude holes, to 8.73 in bright areas, has also been inferred. *INDEX TERMS:* 7509 Solar Physics, Astrophysics, and Astronomy: Corona; 7511 Solar Physics, Astrophysics, and Astronomy: Coronal holes; 2169 Interplanetary Physics: Sources of the solar wind; 2164 Interplanetary Physics: Solar wind plasma; *KEYWORDS:* SOHO-Ulysses quadrature, low-latitude solar wind, oxygen flow speed, proton flow speed, in situ data

Citation: Poletto, G., S. T. Suess, D. A. Biesecker, R. Esser, G. Gloeckler, Y.-K. Ko, and T. H. Zurbuchen, Low-latitude solar wind during the Fall 1998 SOHO-Ulysses quadrature, *J. Geophys. Res.*, *107*(A10), 1300, doi:10.1029/2001JA000275, 2002.

1. Introduction

[2] Solar and Heliospheric Observatory (SOHO)-Ulysses quadratures occur when the SOHO-Sun-Ulysses-included angle is 90°. These offer the opportunity to directly compare properties of plasma parcels, observed by SOHO [*Domingo et al.*, 1995] in the low corona, with properties of the same parcels measured, in due time, in situ, by Ulysses [*Wenzel et al.*, 1992]. We refer the reader to *Suess et al.* [2000] for an extended discussion of SOHO-Ulysses quadrature geometry. Here it suffices to recall that there are two quadratures per year, as SOHO makes its one-year revolution around the Sun. This, because SOHO is at the L1 Lagrangian point, in essentially the same place as the Earth, while Ulysses is in a near-polar ~5-year solar orbit with a perihelion of 1.34 AU and aphelion of 5.4 AU.

[3] We have conducted ~10 SOHO-Ulysses quadrature campaigns. In this paper, however, we report only on the 1998 November/December quadrature, when Ulysses was

[1]Osservatorio Astrofisico di Arcetri, Firenze, Italy.
[2]NASA Marshall Space Flight Center, Huntsville, Alabama, USA.
[3]NASA Goddard Space Flight Center, Greenbelt, Maryland, USA.
[4]Harvard-Smithsonian Center for Astrophysics, Cambridge, Massachusetts, USA.
[5]Department of Physics, University of Maryland, College Park, Maryland, USA.
[6]Department of Atmospheric, Oceanic and Space Sciences, University of Michigan, Ann Arbor, Michigan, USA.

0148-0227/02/2001JA000275

≈17.4° below the equator, off the west limb of the Sun, and at a distance of 5.2 AU. It should be noted that quadrature occurs, of course, at a specific instant in time. But since Ulysses was within 5° of the limb for 10 days, limb observations corresponded closely to the sub-Ulysses foot point on the Sun. If there are changes in coronal morphology that can be identified with corresponding changes in the solar wind, then the uncertainty in the identification of coronal features with Ulysses measurements can be reduced essentially to zero, even with Ulysses at a distance of 5.2 AU.

[4] Quadrature studies provide complementary information to that gained during Whole Sun Month (WSM) campaigns in which an observing campaign is conducted for one full solar rotation of 27 days. The purpose of WSM campaigns is to determine the relationship between coronal phenomena and the solar wind. They use solar wind data from a variety of spacecraft but which have so far not included spacecraft at quadrature locations. There is thus generally a time difference between when limb observations of the corona are made and the time of solar origin for the solar wind plasma measured in situ. WSM campaigns have contributed greatly to the body of knowledge on solar-interplanetary relations, with WSM1 resulting in a *Journal of Geophysical Research* special section [*Galvin and Kohl*, 1999]. By adding results from quadrature campaigns to the WSM body of knowledge, we provide more concise relationships between specific coronal structures and physical parameters and the resulting solar wind, and we are able to place stricter constraints on coronal parameters as a consequence of observing the same plasma in situ.

[5] The only other technique used to observe the same parcel of solar wind plasma at two points is the radial alignments of interplanetary spacecraft. For example, *Thieme et al.* [1989, 1990] took advantage of an alignment between the two Helios probes to study the evolution of plasma parameters with heliocentric distance inside 1 AU. These observations analyze only interplanetary processes and not coronal processes. However, they do not depend on remote sensing, as do coronal observations, which are thus subject to the influence of unknown structures along the line of sight. We minimize line of sight effects here by utilizing data from high in the corona, at 3.5 and 4.5 R_{sun}, for the spectral analysis with Ultraviolet Coronagraph Spectrometer (UVCS) data.

[6] The first quadrature we analyzed, in May 1997, occurred when the wind speed at Ulysses was low and remarkably smooth: 375 ± 25 km/s [*Suess et al.*, 2000] over the entire two-week observing period. Analysis of the morphology of the region where the solar wind originated showed it to lie just inside the edge of a streamer brightness boundary, in a configuration that didn't undergo any major restructuring throughout the campaign. On the contrary, during the December 1998 quadrature SOHO/Large-Angle Spectrometric Coronagraph (LASCO) C2 images show at 2.0–3.0 R_{sun} a transition from a situation where a streamer lay completely north of the Sun-Ulysses direction to a configuration where a streamer lay on and to the south of the Sun-Ulysses direction. As a consequence, the sub-Ulysses foot point on the Sun initially passes through an unstructured, weakly emitting region and, later, lies on the northern border of a bright streamer. There was only one small coronal mass ejection near the Ulysses foot point so that the observed in situ changes were mainly due to solar rotation bringing features across the limb of the Sun.

[7] This situation permits study of low-latitude high- and low-speed solar wind sources. In general, low-latitude sources have been found to be highly variable [*McComas et al.*, 1998], but much of this variability has been attributed to time-dependent phenomena. In the present case it appears that we are analyzing quasi-stationary flow due to an essentially steady streamer source and the low-latitude extension of a polar coronal hole.

[8] SOHO experiments have provided greatly improved and even entirely new data at high latitudes in the corona over the past solar minimum years, so that we have more and better information on electron densities, kinetic and electron temperatures (both of hydrogen and minor ions), and Doppler dimming [*Hyder and Lites*, 1970] in polar coronal holes. Our knowledge of the physical conditions of the regions where low-latitude wind originates is, however, not as good. There are only the recent studies by *Miralles et al.* [2001], *Del Zanna and Bromage* [1999], and *Bromage et al.* [2000]. *Miralles et al.* [2001], in an analysis of UVCS observations of a low-latitude hole, found evidence for a lower oxygen kinetic temperature and outflow speed than in polar holes in the range 1.5 to 3 R_{sun}. This hole extended for ≈30° in longitude and ≈20° in latitude. The equatorial extension of a polar hole, known as the "elephant trunk" during WSM1 (10 August to 8 September 1996), has been analyzed by *Del Zanna and Bromage* [1999], *Dobrzycka et al.* [1999], and by *Bromage et al.* [2000], who found the hole to be superradially expanding from the chromosphere to the corona (up to $r = 2.25\ R_{sun}$), the OVI line widths to be ≈1.5 times larger than in streamers (at $r = 2.25\ R_{sun}$), densities to be about one-third the values found in adjacent quiet regions, and temperatures (from CDS data) on the order of 8. 10^5 K. WIND observations showed the hole to be the source of wind reaching up to between 700 and 750 km s^{-1}, hence it may not be representative of the source regions of equatorial wind.

[9] In this paper we focus on plasma outflows and their changes in the corona, associated with the changing configuration through which the Sun-Ulysses direction crosses, and we establish a relationship between solar wind speed variation in the corona and solar wind speed variation in interplanetary medium. Abundances and temperatures of the coronal plasma are given on the basis of measurements of the same plasma in the corona and in situ at 5.2 AU, distinguishing this analysis from the earlier studies based only on coronal observations.

[10] The paper is organized as follows: In section 2, LASCO/C2 images are presented, together with ground-based data, to put the quadrature observations into a global context. Section 3 is the analysis of UVCS data: Qualitative results on the behavior of plasma are derived from Lyman-α (section 3) and OVI lines (section 3.1). Ulysses data from the solar wind plasma instrument SWOOPS (Solar Wind Observations Over the Poles of the Sun), ion composition instrument SWICS (Solar Wind Ion Composition Spectrometer), and vector magnetometer VHM/FGM (Vector Helium Magnetometer and Fluxgate Magnetometer) are described in section 4 and then, in section 5, we use these to identify values for the coronal physical parameters, which allow us

to reproduce the line intensities observed on 2 days representative of times when "fast" and "slow" wind had been measured by Ulysses. A discussion of our results in section 6 concludes the paper.

2. LASCO/C2 Observations and the Coronal Context

[11] Figure 1 shows LASCO/C2 negative images [*Brueckner et al.*, 1995] taken on 4 days during the Fall 1998 quadrature campaign. The black horizontal line marks the heliographic equator, and the black line pointing southwest of the equator at $-17.4°$ shows the radial direction to Ulysses. We will refer to this direction when describing limb activity. UVCS slit positions at 3.5 and 4.5 R_{sun} during the campaign are shown in Figure 1 (top right). UVCS observations altogether extended over ~9 days, from late on 29 November (Day of Year (DOY) 333) to early on 7 December (DOY 341).

[12] Figure 1 shows the significant changes the west limb of the Sun underwent over the interval of UVCS observations. On 29 November, C2 emission is dominated by a bright streamer, or complex of streamers, in the northern hemisphere, which extends, on 30 November, to higher altitudes and to a wider-latitude interval. Because our observations refer to a southern latitude of $\approx 17.4°$, they show none of this activity. Although over the next 3 days the streamer emission breaks into a complex of bright, thinner structures extending radially outward, the Sun-Ulysses direction is apparently unaffected by these changes, which do not reach southern latitudes. This was still true on 2 December.

[13] On 3 December enhanced white light emission began to appear south of the equator and a small coronal mass ejection (CME) occurred at the sub-Ulysses point at 21:30 UT on 4 December. By 5 December the emission appeared as a dense streamer. It had started as a cluster of streamers adjacent to each other on 3 December, spanning a large-latitude interval. These increased in brightness over subsequent days and, at the time of the CME, coalesced into one bright feature. The Sun-Ulysses direction no longer went through weakly emitting areas by 5 December, but through the northern edge of this bright feature.

[14] The dim region in the UVCS field of view at 4.5 R_{sun} on the 4 days of 29 November through 2 December is interpreted as a coronal hole. This is consistent with UVCS intensities, LASCO intensities, and the resulting solar wind plasma, abundance, and ionization state properties measured at Ulysses, as we show in subsequent sections. It is also consistent with the ground-based observations of the Mauna Loa Solar Observatory (MLSO) Mk3 K-Coronameter, the Wilcox Solar Observatory (WSO) potential field-source surface model of the coronal magnetic field, and the Sacramento Peak National Solar Observatory FeXIV emission on the west limb. Figure 2 shows the FeXIV data in a synoptic map of east and west limb data at 1.15 R_{sun} from Carrington Rotation 1943. Coronal holes are indicated by white areas bordered by black. Superimposed is a horizontal gray bar covering longitudes 172° to 310° and southern latitudes $-14°$ to $-20°$. This bar, which is 90° west of the central meridian, marks the sub-Ulysses foot point on the Sun at $-17.4°$ latitude over the interval of UVCS observations. It is clear this foot point lies entirely north of the equatorial extension of the south polar coronal hole in FeXIV from 29 November through 2 December (DOY 333 through 336). The implication is that the equatorward boundary of the coronal hole, which is at approximately

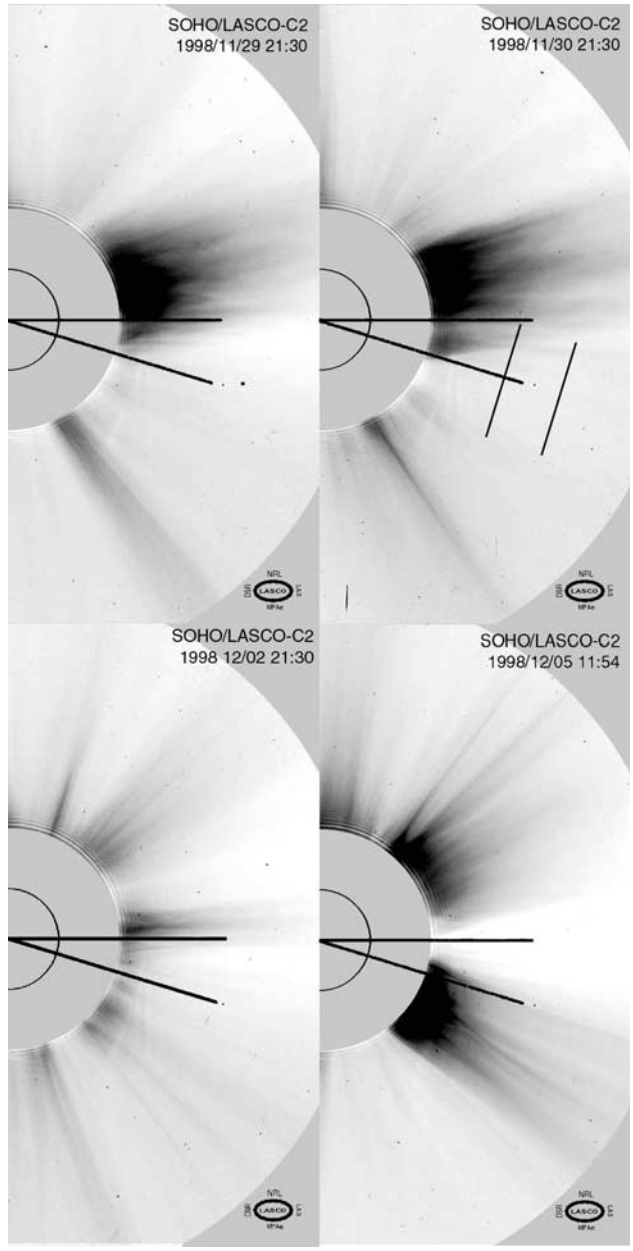

Figure 1. SOHO/LASCO C2 negative, contrast-enhanced images of the west limb of the Sun on 4 days representative of the different conditions met along the directions Sun-Ulysses, at the time of the November/December SOHO-Ulysses quadrature. The inner circle defines the limb of the Sun, the edge of the gray circle gives the size of the C2 occulting disk, and the outer circle is at ~6 R_{sun}, the outer edge of the aperture. The solar equator and the Sun-Ulysses direction 17.4° south of the equator are shown by the black lines from the center of the image, and the locations of the UVCS observing slit are shown in Figure 1 (top right) by the thinner black lines crossing the direction to Ulysses at 3.5 and 4.5 R_{sun}.

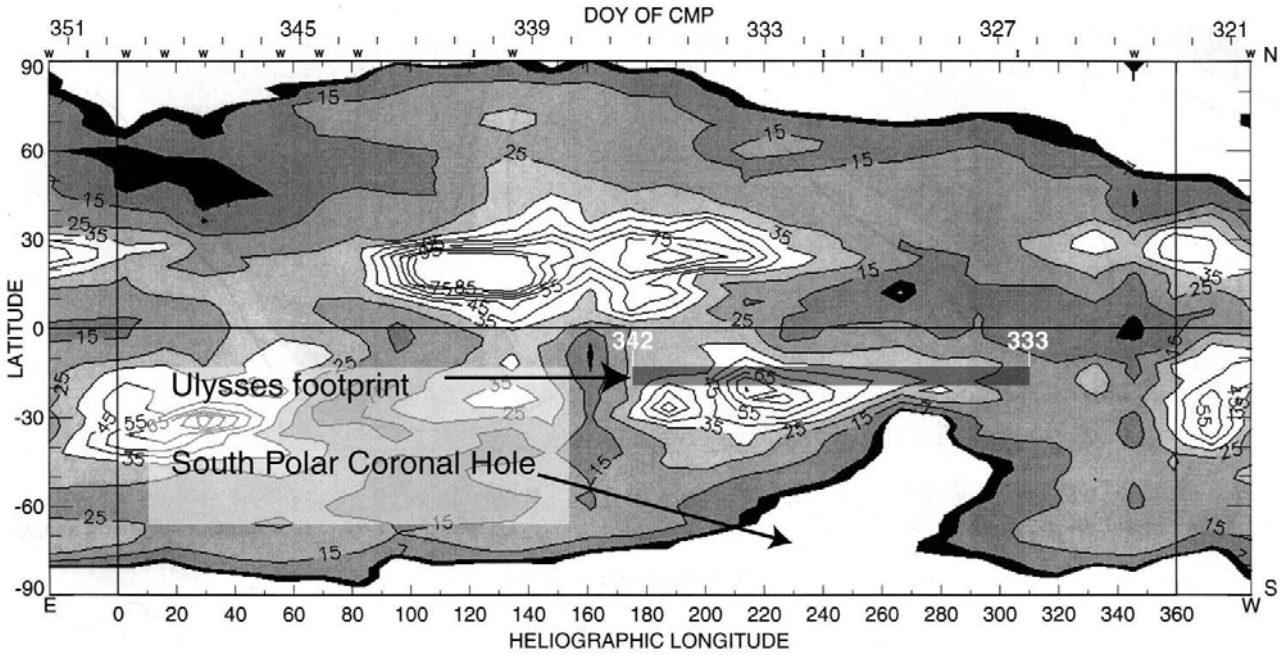

Figure 2. NSO/Sacramento Peak Fe XIV map for Carrington rotation 1943, covering the November/December 1998 days when the Ulysses-SOHO quadrature observations have been made. The data are E + W limb contours: 5, 7, 15, 25, 35, 45, 55, 65, 75, 85, and 95 millionths of I_o at 1.15 R_{sun}. Coronal holes are shown as white bordered by black. The Ulysses foot point, 90° west of central Earth central meridian passage (CMP), is shown as a gray bar extending 3° north and south of the foot point. The beginning and ending DOY are shown above the gray bar.

$-30°$ at 1.15 R_{sun}, diverges both in the east-west direction and toward the equator between longitudes 250° and 300° so that it is north of the direction to Ulysses and $\geq$4 days in width at the UVCS slit position. In Figure 1 this boundary can be seen to be diverging at 2.0 R_{sun} in precisely the suggested manner. Inspection of this boundary in MLSO data shows it to also be diverging. The WSO source surface field shows the heliospheric current sheet as extending far north of Ulysses during this time. The divergence is consistent with MHD models of coronal dynamics [e.g., *Neugebauer et al.*, 1998; *Linker et al.*, 1999] but seems to contradict the lack of such divergence proposed by *Woo et al.* [1999]. From the images in Figure 1 it is difficult to tell whether the flow is already radial at 3.5 R_{sun}, but the appearance is consistent with radial flow at and beyond 4.5 R_{sun}. The width of the fast and slow wind regions originating from these structures is consistent with radial flow beyond 4 R_{sun}.

[15] We surmise that observations acquired during the first days of the quadrature campaign refer to the limb passage of the equatorial extension at 2–5 R_{sun} of the south polar coronal hole, even if it doesn't reach, at the coronal level of FeXIV maps, the latitude of 17.4°, through which the radial to Ulysses crosses. If our hypothesis is correct, we expect the earliest UVCS observations, taken late on 29 November, to be representative of plasma from the western edge of the hole. A similar situation will hold for the following $\approx$4 days that it takes the coronal hole to rotate past the limb of the Sun.

[16] The bright region trailing the coronal hole, in the Sacramento Peak FeXIV data of Figure 2, shows up at higher altitudes, in LASCO images, as the streamer complex we described. If, as generally claimed, the source of slow wind is related to streamers [e.g., *Gosling et al.*, 1981; *Sheeley et al.*, 1997; *Habbal et al.*, 1997], we expect at these times a slower plasma outflow than observed on the previous days. In section 3 we analyze UVCS data to check whether the information they convey complies with the qualitative picture emerging from LASCO and Sacramento Peak maps.

3. UVCS Observations

[17] UVCS observations during the 1998 quadrature were made with the same plan used during the 1997 quadrature campaign [*Suess et al.*, 2000]. From 29 November to 7 December 1998, we acquired data over $\sim$9 hours per day, alternating between altitudes of 3.5 R_{sun} and 4.5 R_{sun}, typically observing 5400 s at the higher altitude and 2700 s at the lower. Each observational run is made up of 5-min exposures to enable isolating temporal variations whenever the count rates, over that limited time, are high enough to be statistically significant. The slit, 100 μ wide, was set normal to the solar radius, with the radial to Ulysses going through its zero position. Data have a spectral binning of 2 pixels (0.1986) and a spatial binning of 3 pixels (21 arcsec); standard calibration procedures and corrections for flat field effects have been applied [*Gardner et al.*, 1996]. There was no need for stray light corrections at the heights we were observing.

[18] The UVCS spectra covered a number of lines. The brightest line is the hydrogen Lyman-α; the OVI doublet lines at 1032 and 1037 Å, the most intense after Lyman-α, easily being a factor 100 weaker. Hydrogen Lyman-β and the

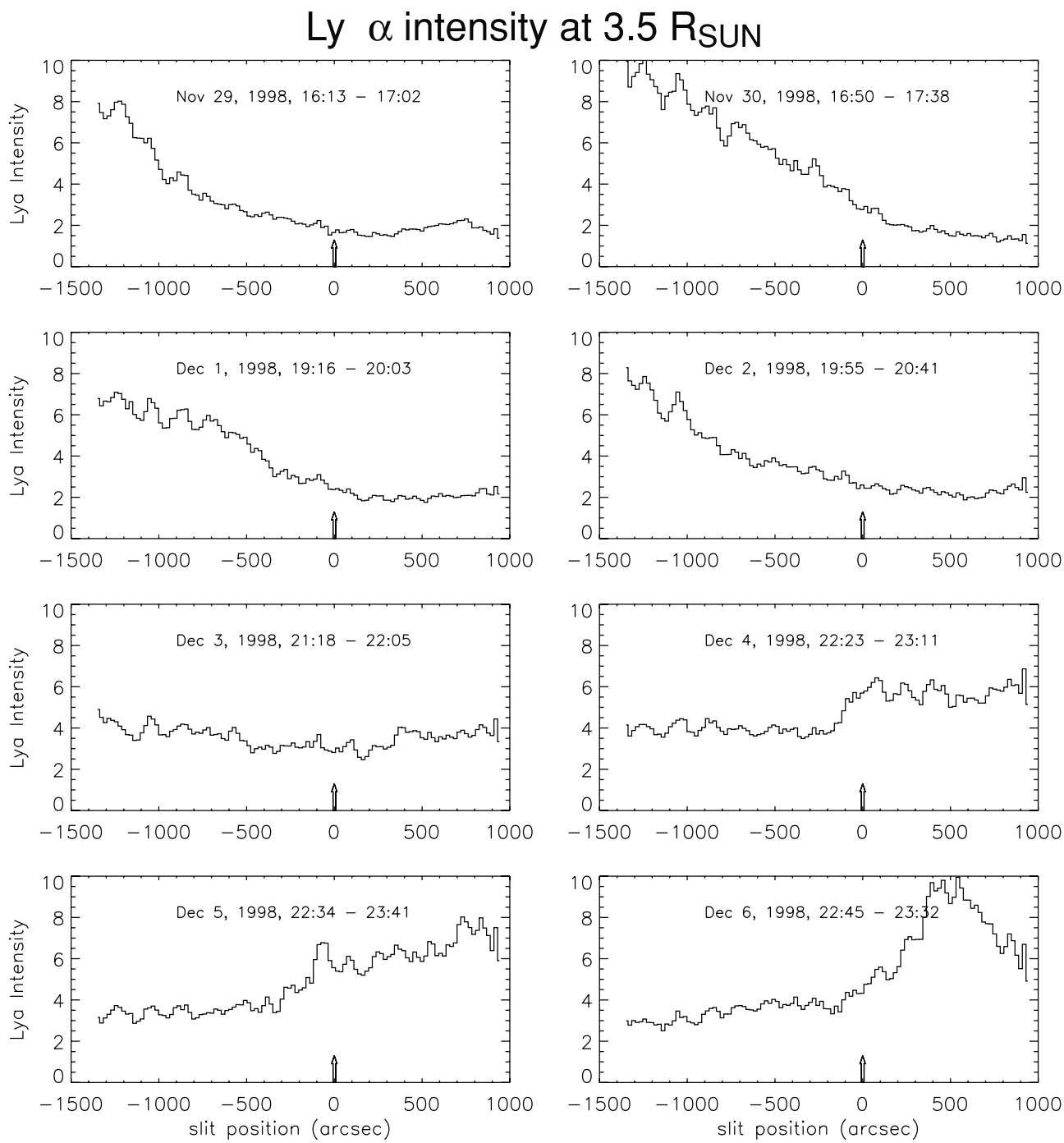

Figure 3. UVCS Lyman-α intensity profile along the slit, during 8 days of the SOHO-Ulysses quadrature campaign, from observations at 3.5 R_{sun}. Units along the abscissa are given in arcsec, the zero position (see the arrow) lying along the radial through Ulysses; north is on the left (negative abscissa values). Units along the ordinate axis are in 10^9 ph cm^{-2} sr^{-1} s^{-1}. The transition from streamer activity north of the Sun-Ulysses direction (negative slit values) to streamer activity along and south of the Sun-Ulysses direction (positive slit values) is clear from Figure 3.

Si XII line at 520.66 Å also were detected, but in the present work we focus only on hydrogen Lyman-α and OVI lines.

3.1. The Lyman-α Line

[19] The total intensity of the Lyman-α line is derived by integrating in wavelength over the line profile and summing over the 5-min exposures, which make up individual observations. The changing morphology at the west limb of the Sun, illustrated in section 2, shows up clearly in the spatial profile of the Lyman-α intensity along the slit given in Figure 3. Each panel in this figure shows the average Lyman-α intensity over one of the 2700-s time intervals at 3.5 R_{sun}, and the arrow gives the position, along the slit, of the radial to Ulysses. Altogether similar plots can be

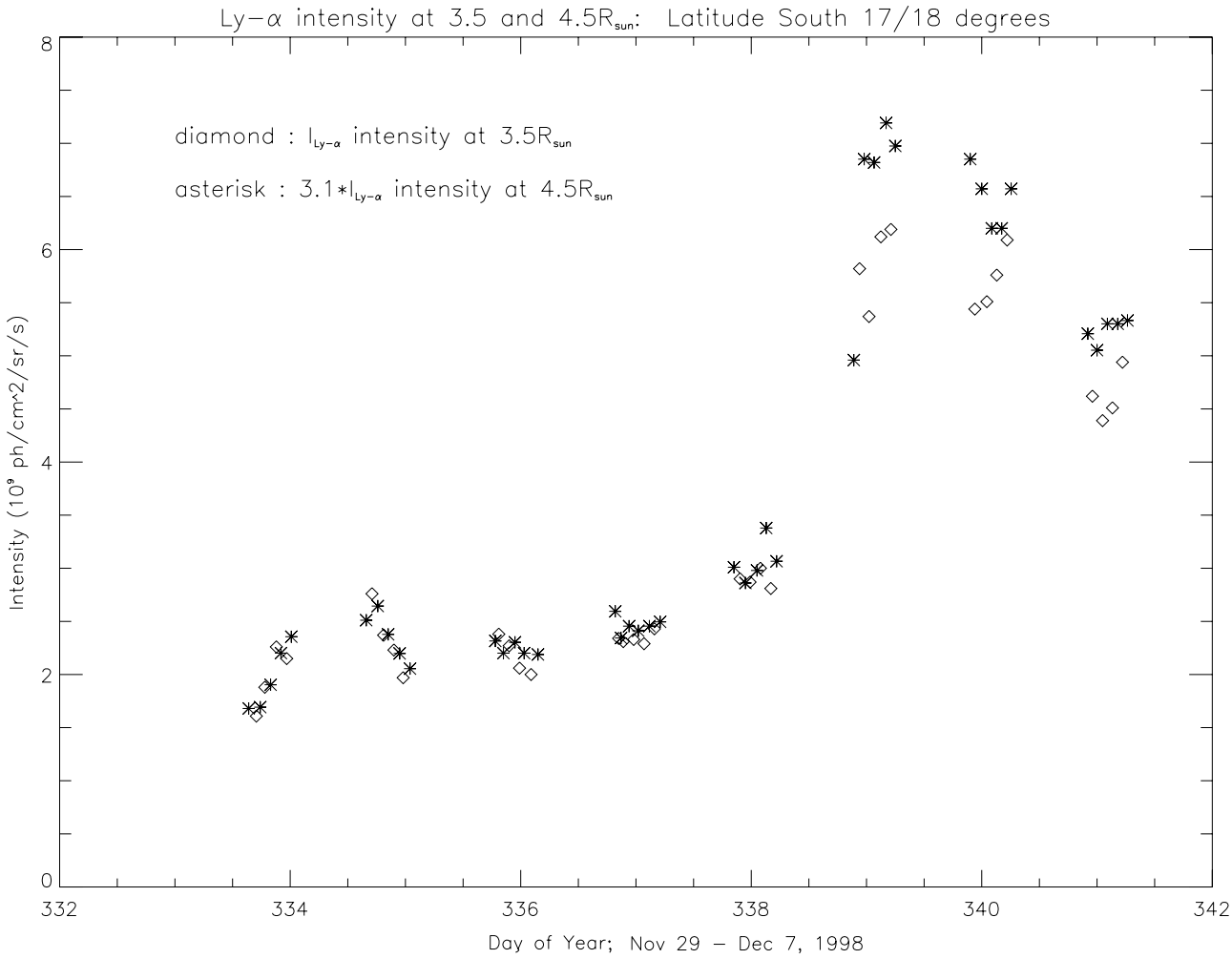

Figure 4. Lyman-α intensity versus time, from 29 November to 7 December, measured by UVCS at 3.5 (diamonds) and 4.5 (asterisks) R_{sun}, along the radial to Ulysses. The plotted intensities have been averaged over pixels included in about 1°, about the radial to Ulysses. Values at 4.5 R_{sun} have been multiplied by 3.1 to facilitate the comparison between the intensity behavior at the two altitudes. Data have been averaged over 2700 and 5400 s, at 3.5 and 4.5 R_{sun}, respectively.

constructed at 4.5 R_{sun}. The transition, from streamer activity north of the Sun-Ulysses direction to streamer activity along and south of the Sun-Ulysses direction, is quite obvious: The Sun-Ulysses direction runs through dark emitting areas until, on 4 December, it cuts through the streamer edge.

[20] Another way to illustrate the behavior of the Lyman-α line is shown in Figure 4, which gives the temporal profile of the Lyman-α line intensity, averaged over a number of pixels corresponding to an angular extent of 1°, about the radial to Ulysses. Values at 4.5 solar radii have been multiplied by 3.1. The plot shows that the Lyman-α intensity increases by a factor ≈3 at DOY 338 (4 December) but also reveals that the ratio between intensities at 3.5 and 4.5 R_{sun}, $I_{Ly\text{-}\alpha,@3.5}/I_{Ly\text{-}\alpha,@4.5}$, is 3.1 during the first days of observations and later on is lower than 3.1.

[21] In order to interpret this behavior in terms of the physical parameters of the regions where the Lyman-α line originates, we need to remind the reader that the line is, at the heights we observe, radiatively excited and that the total (i.e., integrated over the line profile) Lyman-α intensity, as observed along the direction **n** is given by

$$I_{Ly-\alpha} = \frac{hB_{12}\lambda_0}{4\pi} \int_{-\infty}^{\infty} N_1 dx \int_{\Omega} p(\varphi) d\omega' \int_0^{\infty} I_{chrom}(\lambda, \mathbf{n}') \cdot \Phi(\lambda - \lambda_0) d\lambda, \quad (1)$$

where h is Planck's constant; B_{12} is the Einstein coefficient for the line; λ_0 is the rest value for the central wavelength λ of the Lyman-α transition; N_1 is the number density of hydrogen atoms in the ground level; the unit vector **n** is along the line of sight x, and the unit vector $\mathbf{n}'$ is along the direction of the incident radiation; $p(\varphi)\, d\omega'$, where ω' is the solid angle around $\mathbf{n}'$, is the probability that a photon travelling along the direction **n** was travelling, before scattering, along the direction $\mathbf{n}'$; Ω is the solid angle subtended by the chromosphere at the point of scattering; I_{chrom} is the exciting chromospheric radiation, and Φ is the coronal absorption profile.

Table 1. Electron Densities (n_e) From LASCO pB Data[a]

Structure	r = 3.5 R_{sun}	r = 4.5 R_{sun}
Coronal Hole	1. 10^5	4. 10^4
Streamer	2.35 10^5	8.5 10^4

[a] Densities are in cm^{-3}.

[22] In a more concise way we can rewrite the previous equation as

$$I_{Ly-\alpha} \approx const \times \int_{-\infty}^{\infty} f(T_e)F(v, T_k)N_e dx, \quad (2)$$

which shows that the line intensity depends on density, electron temperature, plasma outflow speed, and disk intensity (which is included in the *const*), T_k being constrained by the line width. Because of Doppler dimming, $I_{Ly\text{-}\alpha}$ decreases as the plasma outflow speed increases (all other parameters being equal). Hence if the scenario outlined in section 2 were correct, the higher $I_{Ly\text{-}\alpha,@3.5}/I_{Ly\text{-}\alpha,@4.5}$ ratio observed in the first days of observations would be explained by a higher outflow speed gradient in the coronal hole than in the streamer observed later on.

[23] However, let us first check whether the behavior of $I_{Ly\text{-}\alpha}$ during the quadrature campaign can be explained in terms of density, temperature, and disk intensity in atmospheres with no plasma outflows. Assuming that plasma outflows are negligible (or do not change on DOY 333–342) and that T_e and I_{chrom} are approximately constant with time, we may attempt to interpret the data of Figure 4 only in terms of density versus height and density versus time.

[24] Because the white light emission depends on the electron density, we know from LASCO/C2 in Figure 1 that densities increase between DOY 333 and 337 and DOY 338 and 342, accounting for the increase in Lyman-α emission with time shown in Figure 4. However, electron density versus height profiles, derived via a Van de Hulst inversion of the LASCO/C2 polarization-brightness (pB) data, for $r \geq$ 3.5 R_{sun}, show that the $n_{e,@3.5}/n_{e,@4.5}$ ratio is, in the second half of the campaign (streamer region), greater than or equal to that at earlier times (coronal hole region), as illustrated by Table 1 and in contrast with the behavior of the $I_{Ly\text{-}\alpha,@3.5}/I_{Ly\text{-}\alpha,@4.5}$ ratio. This implies that the Lyman-α behavior depends on other parameters in addition to electron densities.

[25] To eliminate one more variable, we use values of the disk Lyman-α intensity provided by the UARS/SOLSTICE (Solar Stellar Irradiance Comparison Experiment on the Upper Atmosphere Research Satellite) experiment, which gives the average of the whole disk along the Sun-Earth direction. If we make an average over the 7 days before and after the day when data are taken and do this for a typical day in the first half of the campaign and a typical day for the second half of the campaign, it turns out that the disk Lyman-α intensity changes by only a few percent, being higher during the first half of the campaign. As a consequence, I_{chrom} has no major effects on the coronal Lyman-α behavior.

[26] Next we consider whether a change in electron temperatures, from streamers to coronal hole conditions, may explain the observed behavior of the Lyman-α intensity versus height and time. To this end we recall that the electron temperature, T_e, in streamers at 3.5 R_{sun} (and higher), is poorly known. The only estimate above the low corona is that by *Fineschi et al.* [1998], who found $T_e = 1.1\ 10^6$ K $\pm$ .25 10^6 K at 2.7 R_{sun}, a value that is in approximate agreement with the values found by *Gibson et al.* [1999] for the scale height temperatures of streamers during WSM1. Values on the order of 8.5 10^5 K at 3.5–4.5 R_{sun} are compatible with both the *Fineschi et al.* [1998] estimate and the *Gibson et al.* [1999] values.

[27] Electron temperatures in coronal holes at altitudes $\geq$3.5 R_{sun} are even less well known. *Ko et al.* [1997], in a study based on ion charge states from measurements made in situ with SWICS [*Gloeckler et al.*, 1992] in the fast wind from a south polar coronal hole, give $T_e \sim 7.3\ 10^5$ K at 3.5 R_{sun}, which is $\sim$10% lower than the streamer temperature given above. Two-fluid models of coronal holes [*Habbal et al.*, 1995] give $T_e \sim 9.\ 10^5$ K at the same height. Hence coronal hole electron temperatures are approximately equal to or lower than streamer electron temperatures at this height.

[28] If we take the interval 7.3 10^5 K $\leq T_e \leq$ 9. 10^5 K as an indication of the T_e variation to expect at 3.5 R_{sun}, we anticipate minor fluctuations in the Lyman-α intensity as a consequence of a change in the electron temperature from "typical" streamer to coronal hole values (the H^{+0} ion abundance changes by $\approx$30% between these two temperatures).

[29] We conclude that unless we invoke a contrived behavior for T_e versus r and for the change of T_e from coronal holes to streamers, unsupported by any evidence, this discussion leads us to invoke a change in the plasma outflow speed if we want to understand the behavior of the Lyman-α intensity versus time and height. We now turn to the analysis of OVI lines to determine whether the conclusions we draw here are consistent with OVI ion behavior.

3.2. The OVI 1032 and 1037 Doublet Lines

[30] OVI lines provide, through the ratio of their total intensities, a proxy for plasma outflow speed [*Noci et al.*, 1987]. In first approximation, we may say that the lower the ratio R of the total intensity of the 1032 Å to the 1037 Å line, where $R = I_{1032}/I_{1037}$, the higher is the plasma outflow speed. This ratio does not depend on oxygen abundances and disk intensities; it is insensitive to T_e [*Li et al.*, 1998], and for a given density it is a function of the plasma outflow speed.

[31] Figure 5 shows the profile of R versus time on DOY 333–342 derived from measured OVI line intensities at 3.5 and 4.5 R_{sun}. The OVI line intensity has been averaged over the pixels lying within 1° about the radial to Ulysses, as we did for the Lyman-α line. Values at 3.5 R_{sun} are higher than those at 4.5 R_{sun}, as expected because of lower outflow speeds at lower heights. Moreover, in reference to the scenario we described in the previous section, values during the first part of the campaign point to a plasma outflow faster than on later days. The transition occurs at $\approx$DOY 338, that is, on $\approx$4–5 December, when the radial to Ulysses leaves the dark area and crosses into the streamer region, in agreement with the conclusions we made on the basis of LASCO/C2 data in section 2.

[32] Because we have densities derived from LASCO/C2 pB data, and R is insensitive to other parameters, including T_e, we may build R versus outflow speed (V_{OVI}) curves and find the OVI outflow speed that fits the observed ratios. As typical values we need to reproduce, we separately choose the average of R over all the data points before or after the transition from lower to higher R values in Figure 5. We thus end up with four values which represent, at 3.5 and 4.5

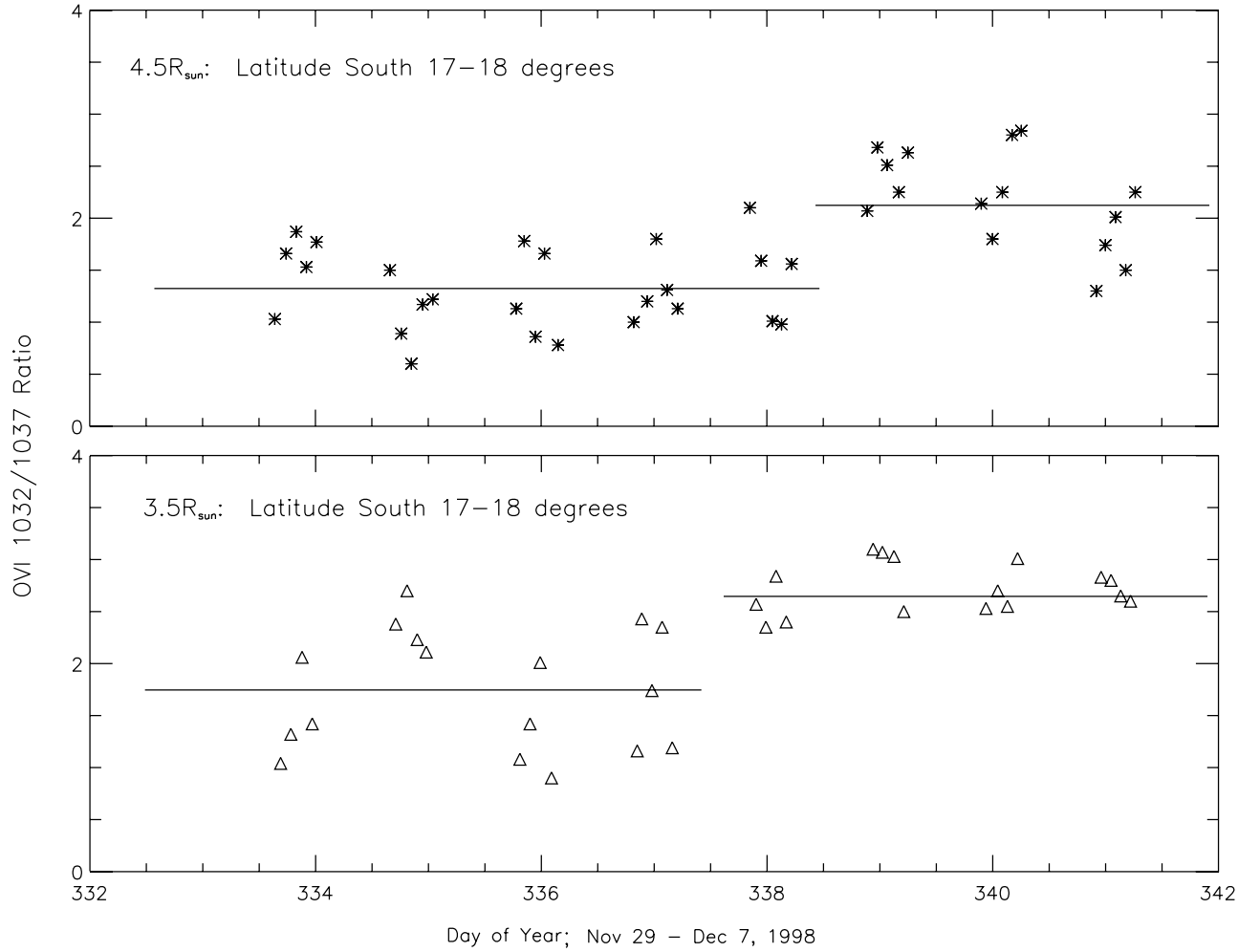

Figure 5. UVCS OVI I_{1032}/I_{1037} Å ratio at (top) 3.5 and (bottom) 4.5 R_{sun} versus time, from 29 November to 7 December. R values have been averaged over pixels included in about 1°, about the radial to Ulysses. A transition to high R values occurs at DOY 338–339, hinting to a decrease of the OVI ions outflow speed. Data have been averaged over 2700 and 5400 s, at 3.5 and 4.5 R_{sun}, respectively. Horizontal lines are drawn at ratios corresponding to the average values of R over bright and dark regions.

R_{sun}, typical "dark" and typical "bright" equatorial regions. We note in passing that the steep transition to higher R values possibly occurs at 3.5 R_{sun} earlier than at 4.5 R_{sun}, hinting there is a coronal hole which is not as wide in longitude at 3.5 R_{sun} as at 4.5 R_{sun}.

[33] Typical "dark" area values turned out to be, at 3.5 and 4.5 R_{sun}, R = 1.73 and R = 1.32, respectively; typical "bright" area values are, at 3.5 and 4.5 R_{sun}, R = 2.65 and R = 2.15, respectively. These are the values we need to reproduce, in order to derive values for the outflow speed of OVI ions. Before describing the results of our simulations, it is worth pointing out that, during the May 1997 quadrature campaign, when Ulysses was immersed in slow wind from the streamer belt, we found R to be 2.69 and 2.24, at, respectively, 3.5 and 4.5 R_{sun}, essentially the same as the values derived in the present campaign in "bright" areas. Values in dark areas are higher than those given by *Cranmer et al.* [1999] in polar coronal holes (R =.95 at 3 R_{sun}) but are consistent with those of *Miralles et al.* [2001] for equatorial holes (R = 1.7 at 3.15 R_{sun}), confirming the latter to be sources of lower speed wind than from polar holes.

[34] As we mentioned, the ratio of the total intensity of the OVI 1032 to the OVI 1037 lines depends mainly on densities and OVI outflow speed. However, because OVI lines form both via radiative excitation (analogous to what happens for the H Lyman-α line) and via collisional excitation, other parameters such as T_e and the kinetic temperature, T_k (or, more precisely, its components normal, $T_\perp$, and parallel, $T_\parallel$, to the magnetic field direction), need to be known in order to evaluate $R = I_{1032}/I_{1037}$. The kinetic temperature $T_\perp$ may be derived from the OVI line widths, measured over the same pixels we used for the intensity evaluation. OVI lines are too weak at the altitudes we analyze to allow us to derive a clean profile, unless we make averages over larger spatial extents and longer observing times. Keeping these uncertainties in mind, we derived the OVI 1032 line width by summing over all the observations taken on a single day and analyzing the resulting profile (we couldn't make spatial averages, as the result would not have been representative of the ambient along the radial to Ulysses). It turns out that when the radial to Ulysses was crossing the "bright" areas, the kinetic temperature at 3.5 and 4.5 R_{sun} was, respectively, 1.5 10^7 K and 2.

10^7 K, values which differ by $\leq$ 10% from those given by *Kohl et al.* [1997] for streamer kinetic temperatures.

[35] Kinetic temperature estimates in dark regions are subject to larger uncertainties. The value we derived with the procedure described above leads to $T_\perp \approx 6.8\ 10^7$ K, with hardly any variation with altitude. *Cranmer et al.* [1999] give higher $T_\perp$ for polar coronal holes; our estimate is, however, consistent with values given by *Miralles et al.* [2001] for $T_\perp$ in equatorial holes. The agreement of the kinetic temperatures we derive with values found either for streamers or coronal holes, as appropriate, is a further evidence that UVCS is observing first a hole and, later on, a streamer. In order to build the R versus $V_{\rm OVI}$ curves, we used electron temperatures on the order of 10^6 K and parallel kinetic temperature values in between $T_\perp$ and T_e. We postpone a discussion of these parameters to sections 5.1 and 5.2, as they are not crucial for the R versus $V_{\rm OVI}$ curves.

[36] Results from R versus $V_{\rm out}$ profiles give, as typical values for the OVI plasma outflow speed in "dark" areas, $V_{\rm OVI@3.5\ Rsun}$ = 200 km s^{-1} and $V_{\rm OVI@4.5\ Rsun}$ = 230 km s^{-1}; for plasma outflows in "bright" areas, $V_{\rm OVI@3.5\ Rsun}$ = 65 km s^{-1} and $V_{\rm OVI@4.5\ Rsun}$ = 105 km s^{-1}. These values fully support the conclusion we drew from the qualitative analysis of the Lyman-α that plasma, over the first days of the quadrature observations, flows at higher speed than over the second half of the campaign and support the interpretation of dark areas in terms of coronal extension at low latitudes and of bright areas in terms of streamer plasma.

[37] So far, SOHO data have allowed us to evaluate densities, kinetic temperatures ($T_\perp$), and the OVI ion outflow speed. By using Ulysses in situ data, we can derive other coronal plasma parameters, such as the proton coronal flow speed. With this information, we may model the OVI and Lyman-α line intensities, at 3.5 and 4.5 $R_{\rm sun}$, setting stringent constraints to parameters which, unless in situ data are used, remain ill defined. This will be shown in section 5.

4. Ulysses SWOOPS, SWICS, and VHM/FGM

[38] We would like to relate in situ solar wind plasma and magnetic field data as precisely as possible to their coronal sources and thereby provide quantitative constraints on coronal plasma properties. The mostly low level of solar activity, with the 4 December CME marking the distinct transition from coronal flow to streamer flow, permits this to be done very accurately. The first step is to extrapolate the in situ properties back to the Sun, which will be done in two ways.

[39] Figure 6 shows the 1-hour averaged proton flow speed, proton temperature, and proton and alpha particle densities from SWOOPS, the 1-hour averaged east-west magnetic field (B_ϕ) from VHM/FGM, and the 3-hour averaged O^{7+}/O^{6+} density ratio from SWICS. The dates at Ulysses are marked across the top of the plot. In making the extrapolation, we will assume radial flow. This is invalid below 2.5 $R_{\rm sun}$ because of the diverging flow but appears valid above 3.5–4.5 $R_{\rm sun}$ because the fast wind stream in Figure 6 is 3–4 days wide, and the high speed flow at 4.5 $R_{\rm sun}$ deduced from UVCS above is also 3–4 days wide. Equal widths are also found for the slow wind at 4.5 $R_{\rm sun}$ and at Ulysses. We will use the difference in size of the coronal hole at 1.15 $R_{\rm sun}$ in Figure 2 and at 4.5 $R_{\rm sun}$ and

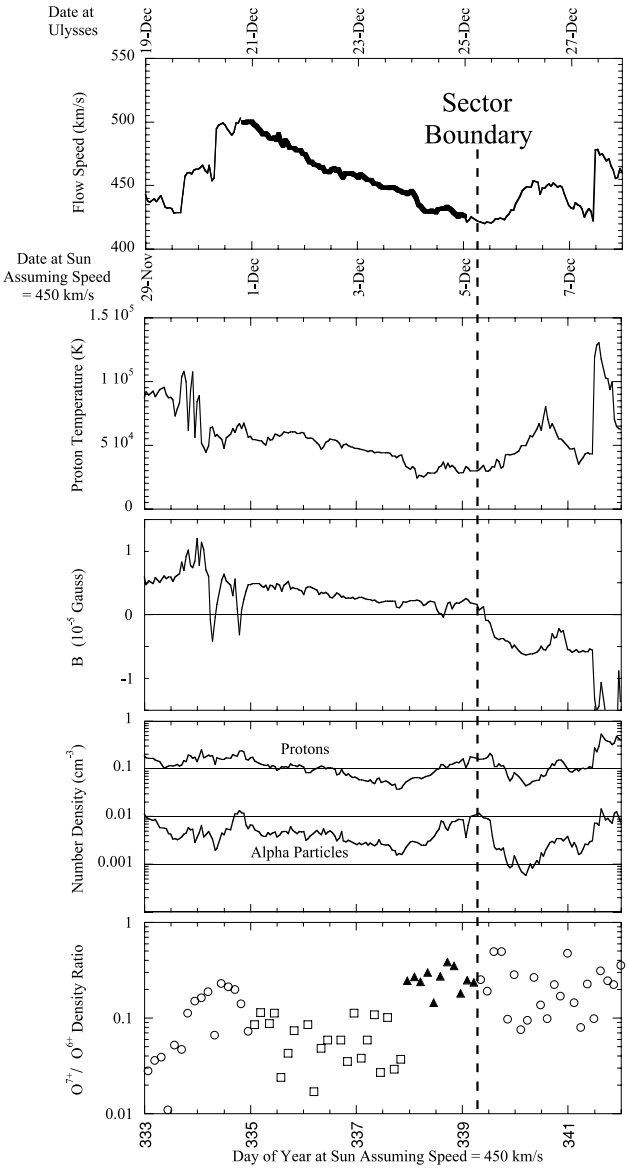

Figure 6. Ulysses SWOOPS measurements of the proton flow speed, proton temperature, and number density of protons and alpha particles, VHM/FGM measurements of B_ϕ, and SWICS measurements of the O^{7+}/O^{6+} density ratio. The time interval corresponds to the expected arrival time of the plasma at Ulysses for the November/December SOHO-Ulysses quadrature. Assuming a solar wind plasma speed of 450 km s^{-1}, the extrapolated origin date is shown at the bottom of the first panel, and the origin day of year is shown on the bottom of the fifth panel.

Ulysses to estimate the amount of divergence, or spreading factor, in the flow. There can also be significant exceptions to the assumption of radial flow at the front of corotating interaction regions (CIRs) [*Gosling and Pizzo*, 1999; *Pizzo*, 1994]. The interaction region in Figure 6 is at the front of the fast wind interface, on 19 and 20 December 1998, which we will avoid in our analysis.

[40] The transit time of each solar wind parcel to Ulysses depends on the speed of that parcel, which, in turn, is generally not a constant so that a quantitative extrapolation

is an impossible inverse, nonlinear problem. However, simple approximations can be used and then fine-tuned by matching with the observed coronal structure. The simplest extrapolation is to map an interval of solar wind plasma back to the Sun using the average measured speed of the plasma. The average speed on 19–27 December 1998 was 450 km s^{-1}. Combining this with the instantaneous distance to Ulysses gives the origin dates shown in Figure 6 (first panel, bottom) for an extrapolation back to 1 R_{sun}. The corresponding DOY is shown along the bottom of Figure 6, and we will use the DOY when referring to specific dates and time intervals.

[41] In Figure 6 (first panel) the "dwell" in the fast solar wind, beginning just after the CIR, is highlighted. The dwell is a dynamic rarefaction region [*Gosling and Pizzo*, 1999; *Pizzo*, 1994] for which relatively precise backward extrapolations can be carried out [*Neugebauer et al.*, 1998]. The speed and density in a rarefaction always fall from their peaks just after the CIR, on the back side of the fast wind stream. The extrapolation for v = 450 km s^{-1} suggests the fast wind originated at the Sun on DOY 335–338, centered at ~DOY 337. The proton temperature is $\sim 5 \times 10^4$ K except near the end of the dwell, and the sector boundary, just after the end of the dwell on DOY 339.3, is unusually distinct. The proton number density is 0.15 cm^{-3} at the beginning of the dwell and decreases until it reaches a minimum on ~DOY 337. This is typical of a rarefaction, and 0.1–0.15 cm^{-3} scales to 2.7–4.0 cm^{-3} at 1 AU. All of these properties are typical of flow from a small, equatorial coronal hole [*Neugebauer et al.*, 1998]. The O^{7+}/O^{6+} density ratio is relatively low from DOY 335 to the beginning of DOY 338, indicative of coronal hole flow because of the generally lower electron temperature in coronal holes. The large variability in this ratio is a real effect [*Aellig et al.*, 1999], which we suggest is due to the highly filamentary nature of coronal hole flow [*Suess et al.*, 1998].

[42] The other way we extrapolate solar wind back to the Sun is to use the "constant velocity approximation" in which the speed of each sample of plasma is assumed constant for computing the transit time. Applying this extrapolation to the dwell, in particular, generally gives a qualitative estimate of the size of the originating coronal hole. The result of this approximation is shown in Figure 7. The first panel in this figure reproduces that in Figure 6. The second panel is the flow speed extrapolated back to 1 R_{sun}, and the third panel is the extrapolated O^{7+}/O^{6+} density ratio. Figure 7 shows that all of the plasma in the dwell appears to originate from a longitude range at the Sun, which is only 1 day in width. This is the same as the width of the FeXIV coronal hole shown in Figure 2. Figure 7 places the center of the high-speed wind source at ~DOY 337, just as did the extrapolation using v = 450 km s^{-1}. This differs from the location of the coronal hole in FeXIV at DOY 335.5 in Figure 2. The FeXIV coronal hole coincides with the dim regions in LASCO/C2 and UVCS data, so we are assured this is the true location of the hole. Therefore we deduce that the extrapolation back to the Sun using either v = 450 km s^{-1} or the constant velocity approximation requires an additional ~20° of rotation, or 1.5 days, to match with the observed morphology. *Neugebauer et al.* [1998] found that an additional 22° of rotation had to be added, on the average, to extrapolations from Ulysses back to 2.5 R_{sun} in a study of

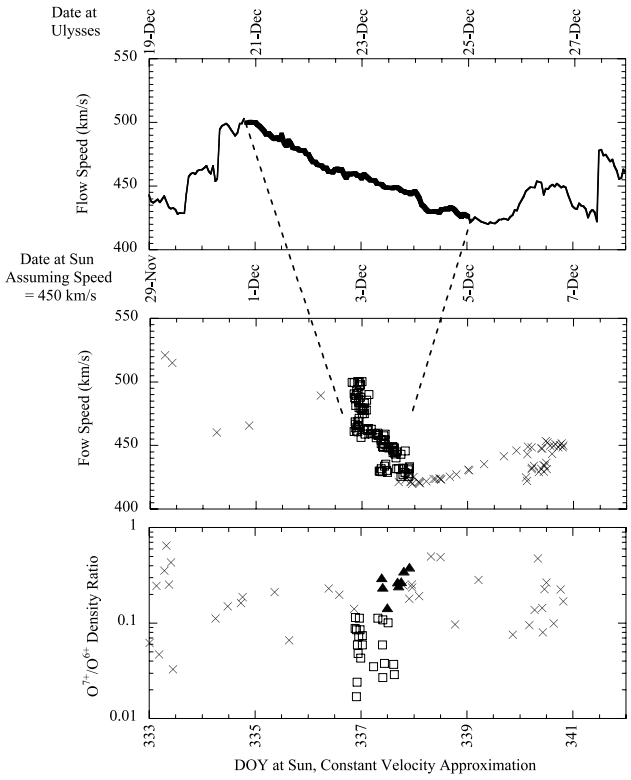

Figure 7. The first panel shows Ulysses SWOOPS proton speed from Figure 6 (first panel). The second panel shows speeds extrapolated back to the Sun making the constant velocity approximation. The third panel shows SWICS O^{7+}/O^{6+} density ratio extrapolated to the Sun using the constant velocity approximation. The origin dates are shown as DOY at the bottom of the third panel. Plasma in the dwell of the fast wind stream is highlighted in the first panel. This same data is plotted as boxes in the second panel to show that all of the plasma in the dwell originates from the same narrow band of longitudes on the Sun, the coronal hole. The O^{7+}/O^{6+} density ratio data in the dwell is plotted as boxes or filled triangles depending on whether the ratio is typical of fast wind or slow wind.

source regions for the solar wind during the Ulysses "fast latitude scan" in 1994–1995. They attributed this additional rotation to a failure of the extrapolation to accurately take into account solar wind acceleration near the Sun, and the adjustment should be approximately the same for the November/December 1998 quadrature. The time difference in extrapolating to 2.5 or 1.0 R_{sun} is <1 hour so the 1.5 day adjustment in the extrapolation that we find, to match with coronal morphology, is supported by independent evidence, and we have identified and separated the coronal sources of fast and slow wind with considerable confidence.

[43] One observation we can make from Figure 7 is that all of the solar wind plasma in the dwell appears to originate from the same 1-day range in longitude at the Sun. This apparently includes a portion of plasma with enhanced O^{7+}/O^{6+} density ratio $\equiv R_O$, which has been identified with filled triangles, as well as the low R_O value plasma plotted as open squares. A low R_O would normally be used to identify coronal hole as this correlation has been well documented with Ulysses/SWICS using data from inside

2.2 AU [*Geiss et al.*, 1995]. Doing this for the data in Figure 6 would imply the boundary between coronal hole and streamer flow occurs at DOY 338.0 at the time of the CME, which is in the dwell on the back of the fast wind where there is no obvious alternative way to separate coronal hole flow slow wind. The constant velocity approximation implies that all the plasma from the dwell originated from the same narrow range in longitude, including some of the plasma with an elevated R_O. The simplest interpretation is that the plasma on DOY 338.0–339.3 in Figure 6 comes from the small and slow (300 km s^{-1}) CME that actually occurred on DOY 338.8. Enhanced O^{7+}/O^{6+} and alpha particle to proton density ratios are strongly associated with CMEs [*Forsyth and Gosling*, 2001; *Galvin*, 1997; *T. Zurbuchen*, personal communication, 2001]. The slight time difference error in the extrapolation can be attributed to slowing of the CME as it moves out into the solar wind, which also has resulted in no speed difference between the ambient and CME material at Ulysses. The result in Figure 7 is sufficient to place the center of the extrapolated coronal hole at DOY 337, which corresponds to the observed coronal hole at DOY 335.5 after the additional 20° eastward shift required by coronal morphology and similar to that described by *Neugebauer et al.* [1998].

[44] Another observation from Figure 7 is that given the spreading of the flow in the east-west direction from 1 day in width at the Sun to 3–4 days in width at Ulysses and assuming a similar expansion equatorward, the local spreading factor for this equatorial extension of the polar coronal hole is ~10. This coronal hole is thus locally a small, rapidly diverging, equatorial coronal hole. *Neugebauer et al.* [1998] found that such coronal holes produce slower solar wind (~500 km s^{-1}), just as seen in Figures 6 and 7, although there could also be slowing of the material between the Sun and 5.2 AU in the CIR [*Pizzo*, 1994]. This is in agreement with the results found from UVCS that indicate lower speeds in the equatorial coronal holes than typically found for the polar coronal holes at solar minimum.

[45] Turning to the slow wind coming from the bright streamer observed with LASCO/C2 and UVCS on DOY 338–442, this corresponds to the flow on DOY 339.5–342 and slightly beyond in Figure 6. There is a small CME at ~DOY 341.5 so we will not consider solar wind flow after that time (the CME occurred later at the Sun and was outside our observation window). The slow wind has a variable speed between 420 km s^{-1} on DOY 339.3 and 450 km s^{-1} on DOY 340.5. The density peaks earlier, at DOY 339.3, at a value of ~0.15–0.20 cm^{-3}. The mass flux at the density peak has been used to define the proton mass flux used in evaluating the UVCS data. Values for R_O throughout the interval DOY 339–342 indicate a slow wind source in the corona.

[46] Finally, the oxygen abundance can be derived by combining He/H from SWOOPS with He/O from SWICS, with somewhat lower time resolution than for the data shown in Figures 6 and 7. The 1-day average values of the ratio of oxygen to proton number density is shown in Figure 8 for DOY 350–365 at Ulysses (16–31 December). The first panel shows the corresponding flow speed derived from alpha particles (solid line) and oxygen (open triangles). The second panel shows the O/H ratio. The corresponding days at the Sun, assuming $v = 450$ km s^{-1}, can be read from Figure 6, and the same 1.5-day (20°) eastward shift applies in Figure 8 as in Figure 6 to match this structure with the coronal morphology. Knowing this, the oxygen abundances on DOY 358 and DOY 361.5 in Figure 8 are used to compute the oxygen mass flux in the corona with UVCS data on DOY 336 and DOY 339. It is worth noticing that the O/H abundances shown in Figure 8 range from 0.0007 to 0.001; that is, they are rather large if we compare them with those measured during mid-1992 and mid-1993 when the O/H ratio for $v_\alpha \leq 500$ km s^{-1} ranged between 0.0002 and 0.0008 [*von Steiger et al.*, 1995]. Because abundances are highly variable [*Aellig et al.*, 1999], this may not be surprising. However, we like to point out that the values we used for our simulations of the OVI line intensities are, in streamer regions, higher than in coronal holes, in agreement with SWICS measurements and in contrast with the behavior of the oxygen abundance in fast versus slow wind, where the higher the speed, the higher the oxygen abundance is. It is interesting to note that having mass fluxes for both oxygen and protons it would be possible to remove the streamline spreading factor between 4.5 R_{sun} and Ulysses from the analysis if necessary.

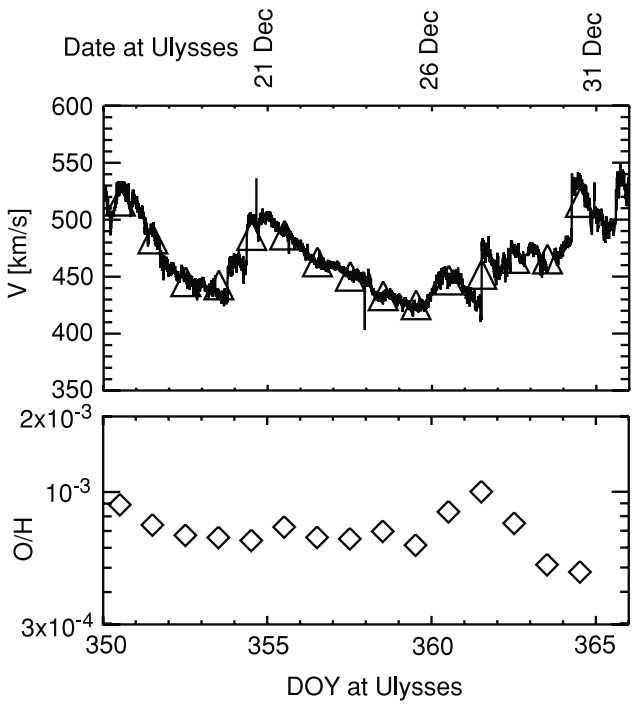

Figure 8. The first panel shows Ulysses SWICS alpha particle speed (solid line) and oxygen speed (open triangles). The second panel shows daily averages of the O/H absolute abundance ratio. The DOY at Ulysses are shown across the bottom of the second panel, and the corresponding dates in 1998 are shown across the top of the first panel.

5. Plasma Parameters in Low-Latitude Coronal Regions

5.1. Low-Latitude Solar Wind From Coronal Holes

[47] We start analyzing data from the first half of the quadrature campaign when we observe the equatorward extension of a polar coronal hole. We focus here on the proton flow speed, v_p, which may be identified by modeling the observed Lyman-α intensity on the basis of known

parameters (density, disk brightness I_{chrom}) and of the value of v_p for which the simulated intensity reproduces observations. Because $I_{Ly\text{-}\alpha}$ depends on other parameters as well, like T_e, this procedure allows us to find a set of parameters compatible with observations.

[48] The Ulysses SWOOPS experiment provides in situ values of the proton density and speed, reducing the number of free parameters. The proton density on 20 December (which is the time when protons leaving the Sun on 2 December reach Ulysses), taken back to 1 AU, is $\sim$4 particles cm^{-3}, and the speed is on the order of 500 km s^{-1}. Hence the mass flux turns out to be $\approx$1. 10^{13} cm^{-2} s^{-1}, and because of mass flux conservation, this value represents the coronal mass flux as well. At 4.5 $R_{\rm sun}$ we may safely assume the expansion to be radial: The *Kopp and Holzer* [1976] superradial expansion, for instance, which *Miralles et al.* [2001] suggest to hold also in equatorial holes, differs by only a few percent from a radial expansion in the interval between 3.5 and 4.5 $R_{\rm sun}$. In this case, it turns out that the proton speed is $\approx$150 km s^{-1} at 4.5 $R_{\rm sun}$.

[49] In order to calculate $I_{Ly\text{-}\alpha}$ with this value of v_p and the known densities and I_{chrom}, we need to fix values for $T_{\|}$, $T_{\perp}$, and T_e. Because the perpendicular kinetic temperature $T_{\perp}$ is constrained by the line width (and plays a minor role in the line intensity calculation for $T_{\perp}$ values measured in equatorial and polar holes), we are left with only two free parameters, T_e and $T_{\|}$ (the latter being less crucial than T_e). As we mentioned, the electron temperature is essentially unknown in equatorial holes. For simplicity, we assume that the T_e versus r profile is the same in equatorial and polar holes. *Cranmer et al.* [1999], in their polar hole model, used the T_e versus r profile of *Ko et al.* [1997], which gives $T_e \approx$ 5.5 10^5 K at 4.5 $R_{\rm sun}$. In this case the computed and observed Lyman-α intensities differ by $\leq$10–15%, depending on whether we assume a constant T_e along the line of sight (which corresponds to assuming hydrogen to be frozen-in at this distance) or T_e to vary along the line of sight with the *Ko et al.* [1997] profile. The parallel kinetic temperature has been assumed to be on the order of 10^6 K, higher $T_{\|}$ leading to higher Lyman-α intensities.

[50] Mass flux conservation implies, at an altitude of 3.5 $R_{\rm sun}$, an outflow speed of $\approx$100 km s^{-1}. However, in order to reproduce the observed intensity within a 20% uncertainty, we need to assume that T_e is $\sim$15% higher than predicted by the *Ko et al.* [1997] profile. This hints at a steeper T_e profile in equatorial than in polar coronal holes.

[51] We may compare the present results with previous analyses of polar and equatorial holes. The *Cranmer et al.* [1999] semiempirical model focuses on polar holes up to 3.5 $R_{\rm sun}$. At that altitude they found proton speeds that range between 200 and 400 km s^{-1}. The wide spread in the proton outflow speed is to be attributed to the wide range of v_p, $T_{\|}$, and $T_{\perp}$ parameters that lead to the same Lyman-α intensity, although some sets of parameters are probably untenable because the mass flux they predict is inconsistent with values measured in situ. If we compare the coronal outflow speed we derived with the coronal outflow speed in polar hole models that complies with mass flux conservation, it turns out that the low-latitude speed is about a factor 2.6 lower than the high-latitude fast wind speed (the mass flux value adopted by *Cranmer et al.* [1999] differs by only 3% from the mass flux measured by Ulysses during the low-latitude hole passage). The low-latitude wind originating from the hole we analyze reaches $\sim$500 km s^{-1}, which is about a factor 1.5 lower than the fast wind from polar holes. Hence the ratio between polar and equatorial wind in the corona is higher than the ratio between polar and equatorial wind at 1 AU, implying that equatorial wind accelerates throughout a longer altitude range in the corona than polar wind does.

[52] The oxygen flow speeds at 3.5 and 4.5 $R_{\rm sun}$ have been derived in section 4. It has still to be proven, though, that those values are compatible with the observed intensities of the OVI lines, because different intensities can obviously result in the same value of R. Hence we also synthesize the OVI doublet lines, adopting the values of densities, of kinetic temperature $T_{\perp}$, and of the outflow speed mentioned earlier. We need also to know the disk intensities in the OVI 1032 and 1037 Å lines and in the CII 1037 and 1036.3 Å lines. Unfortunately, we do not have values for the disk intensities of these lines at the time of the quadrature campaign. Hence we assumed oxygen VI ions to behave as Ne VIII or N V ions, whose increase with time throughout the ascending phase of the present solar cycle has been given by *Schühle et al.* [2000]. The CII intensities have been scaled accordingly. Three parameters, $T_{\|}$, T_e, and the oxygen abundance, are still necessary in order to model the OVI intensities. SWICS, through the O^{7+}/O^{6+} ratio and the O/H versus time profiles, gives us some information on these parameters and shows that T_e and the oxygen abundance are lower during the low-latitude hole passage than at later times. Moreover, because oxygen ions move faster than hydrogen at the coronal heights we observe and, at 1 AU, move at about the same speed, we may assume that the in situ O/H value represents an upper limit to the oxygen abundance at coronal levels.

[53] If the OVI 1032 and 1037 doublet lines are synthesized assuming an electron temperature of 1.3 10^6 K (which corresponds to the freezing-in temperature for O^{7+}/O^{6+} ratio of $\sim$0.08), an oxygen abundance of 8.55, and a $T_{\|}$ of 3. 10^7 K, the modeled and observed OVI intensities differ by <10%, both at 3.5 and 4.5 $R_{\rm sun}$. These parameters comply with the in situ constraints, but an increase of the electron temperature and a simultaneous increase of the oxygen abundance may, a priori, be thought to yield the same OVI intensities. This alternative can be ruled out, because the oxygen coronal abundance has to be about half of the in situ abundance, if we consider that the ratio $(N_O V_O)/(n_H v_H)$ is constant and the ratio between the OVI ion speed and the proton speed in the corona is $\sim$2 (all ions of the same element have been assumed to have the same outflow speed; see *Ko et al.*, 1997). SWICS data give an oxygen abundance of $\approx$8.84: Assuming the coronal oxygen abundance value $(O/H)_{cor} \simeq \frac{1}{2}\,(O/H)_{AU} \pm 20\%$, the oxygen abundance value quoted above can vary only by $\approx$0.05, which would lead to a change in the electron temperature of $\approx$10%. Such a constraint in the range of the physical parameters representative of the OVI outflow from low-latitude coronal holes has been possible only because in situ data from the coronal plasma sampled by SOHO were available.

[54] Oxygen speeds at altitudes up to 3 solar radii have been derived by *Miralles et al.* [2001]. Our values are on the upper limit of the range of values that would be extrapolated from their $V_{\rm out}$ versus r profile. Whether this is to be

ascribed to a difference between the behavior of equatorial hole versus equatorial extensions of polar holes is still an open question. We notice, however, that a variability in wind speed from low-latitude holes has been inferred also from in situ experiments [*Neugebauer et al.*, 1998], and it is not surprising to find the same result at coronal levels.

5.2. Low-Latitude Solar Wind From Streamer Regions

[55] When we calculate the mass flux at Ulysses during the second half of the quadrature, with the purpose of inferring the proton outflow speed in the corona, we obtain a speed much lower than at earlier times. This is due to a combination of two effects: On 5 December, which we consider representative of the conditions at the time the radial to Ulysses was crossing the bright areas, the mass flux at Ulysses is lower than it was on 2 December by a factor $\approx$1.25, and the coronal densities, on 5 December, are higher than at earlier times. As a consequence, the proton outflow speed, at 4.5 R_{sun}, turns out to be on the order of 60 km s^{-1} and, at 3.5 R_{sun}, to be on the order of 35 km s^{-1}.

[56] It is worth noticing that these outflow speeds are 2.5–3 times smaller than the outflow speed at the same altitudes over the coronal hole sampled at earlier dates, but the in situ measurements of the proton speed show it to be only a factor 1.16 lower than during the coronal hole passage. This seems to imply that the region where the wind from streamers gets accelerated is located at larger distances, with respect to fast wind from low-latitude holes.

[57] The Lyman-α intensities from the streamer regions have been modeled, analogously to what we did before, taking into account that the exciting radiation is a little lower than at earlier times, using the appropriate density versus height profile and an electron temperature T_e = 9. 10^5 K, in agreement with our discussion of section 3. Line intensities are reproduced with a 10–15% accuracy. $T_{\|}$ has been chosen between $T_{\perp}$ and T_e: At 4.5 R_{sun} the best agreement with observations is obtained for $T_{\|} = T_e$, but changing to $T_{\|} = T_{\perp}$ varies $I_{Ly\text{-}\alpha}$ by only 10%.

[58] When simulating the OVI doublet line intensities, we need to take into account constraints by in situ observations. The O^{7+}/O^{6+} versus time profile indicates that T_e has to be larger than assumed when synthesizing coronal hole lines, and the O/H versus time profile analogously indicates a larger O/H value than on previous days, an upper limit being on the order of O/H = 0.0009. Hence we chose *log* O/H = 8.73 and T_e = 1.5 10^6 K (which corresponds to the freezing-in temperature for O^{7+}/O^{6+} ratio of $\sim$0.2). On the basis of these parameters, the $V_{OVI@3.5}$ and $V_{OVI@4.5}$ derived in section 3.1, and the measured $T_{\perp}$ values, we have been able to reproduce the observed OVI intensities with a $\leq$ 10% accuracy, assuming $T_{\|}$ to be 1. 10^7 and 2. 10^7 K at 3.5 and 4.5 R_{sun}, respectively.

[59] Results presented in sections 5.1 and 5.2 for outflow speeds are summarized in Table 2 and Figure 9, which shows, for altitudes larger than 3 R_{sun}, values for the wind speed in polar and equatorial holes from the present analysis and from literature, and from low-latitude streamer regions from this work. The plot shows that the proton wind speed from low-latitude holes is, in the corona, about a factor 2.5 lower than in polar coronal holes but is about a factor of 3 faster than in streamer regions. Oxygen ions move faster than protons, independent of the region where they originate from, but still they are slower than in polar holes. Fast OVI ion acceleration seems to occur below 3.5 R_{sun} in low-latitude coronal holes, as the OVI outflow speed levels out between 3.5 and 4.5 R_{sun}. Analogous indications have been found by *Cranmer et al.* [1999] in polar coronal holes.

Table 2. Low-Latitude Wind Speed[a]

Structure	r = 3.5 R_{sun}	r = 4.5 R_{sun}
	Coronal Hole	
Protons	100	150
Oxygen	200	230
	Streamer	
Protons	35	60
Oxygen	65	105

[a] Wind speed is in km s^{-1}.

6. Discussion and Conclusions

[60] The purpose of this paper is to identify the physical parameters in low-latitude coronal regions where plasma sampled by Ulysses experiments originate. The analysis we did allowed us to derive values of densities, outflow speeds, electron temperatures, and oxygen abundances at 3.5 and 4.5 solar radii, which are consistent both with the UV line intensities measured at those levels and with parameters measured by in situ instruments. In the following we list briefly our results and give a more extensive discussion of outflow speeds and electron temperatures in sections 6.1 and 6.2, respectively. The low-latitude slow wind at coronal levels of 3.5 and 4.5 R_{sun} has the following characteristics: (1) It originates from either coronal holes or bright regions overlying streamer structures. The coronal hole expansion factor is on the order of 10 and coronal hole electron densities are about a factor 2 lower than in bright areas. (2) It has a proton outflow speed on the order of 100–150 km s^{-1} in coronal holes and 35–60 km s^{-1} in bright areas. (3) It has an OVI ion outflow speed higher than proton outflow speed by a factor 2 at the lower level and by a factor $\approx$1.5–1.7 at 4.5 R_{sun}. (4) It is accelerated at higher levels and through a more extended region than fast polar wind, independent of the region where low-latitude wind originates. (5) It has kinetic temperatures from OVI line widths that in streamer regions are on the order of 1.5–2 10^7 K and in coronal holes on the order of 6.8 10^7 K. That is, in low-latitude holes the kinetic temperature is lower than in polar coronal holes. (6) It has electron temperatures at the levels we consider, although weakly defined (see section 6.2), lower in coronal holes than in bright regions. (7) It has been assumed to have an anisotropic temperature distribution, with $T_{\|}$ values between T_e and $T_{\perp}$, when synthesizing H Lyman$_{\alpha}$ and OVI doublet line intensities. The anisotropy is larger for oxygen ions, where $T_{\perp}/T_{\|}$ is on the order of 2.2 in coronal holes and on the order of 1.3–1.5 in bright regions. (8) It has oxygen ions frozen-in both in coronal holes and streamer regions, with freezing-in temperatures of $\approx$1.3–1.5 10^6 K, respectively.

6.1. Proton and Minor Ion Outflow Speed in the Low-Latitude Corona

[61] It is well known that low-latitude solar wind is highly variable, but most of the low-latitude wind studies have so far focused on its properties at the large distances sampled by in

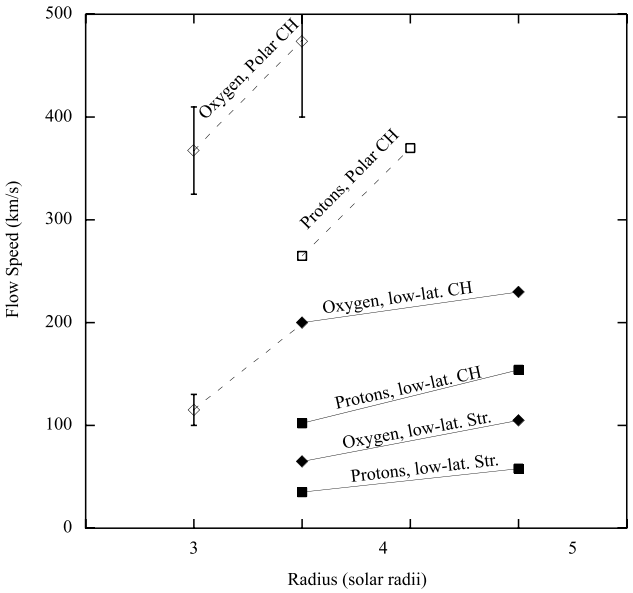

Figure 9. Solid black squares are proton outflow speed at 3.5 and 4.5 solar radii, from the present study, for the 1998 low-latitude streamer and coronal hole we analyzed; solid black diamonds are the same as squares for OVI ions. Open squares are polar proton flow speed from *Cranmer et al.* [1999] minimum corona models. The plotted values comply with mass flux conservation and are calculated with an anisotropic temperature distribution ($T_\perp = T_e$). Open diamonds are oxygen flow speed, in equatorial holes, from *Miralles et al.* [2001] and, in polar holes, from *Cranmer et al.* [1999]. The range of values given by the authors, which correspond to different choices of the free parameter $T_\parallel$ and of other model parameters, are shown in Figure 9. These would be constrained if the oxygen mass flux would be known.

situ instrumentation, while the behavior of the outflow speed at coronal altitudes has been little explored. In this work we present results on this issue starting with the flow geometry. Previous analyses by *Dobrzycka et al.* [1999] and by *Miralles et al.* [2001] had already suggested that equatorial holes expand super-radially: Here we provide further evidence for this, at least for altitudes lower than 3.5 R_{sun}, because wind emanating from the low-latitude extension of the coronal hole we analyzed would not have been sampled by Ulysses, should the flow be radial. We also derived an expansion factor of order 10, which is higher than the usually quoted figures for polar hole flows (which range from 2 to 7.3; see, e.g., *Habbal et al.*, 1995; *Munro and Jackson*, 1977, respectively). That wind from regions with a higher expansion factor has a lower speed (low-latitude holes) than regions with a lower expansion factor (polar holes) is consistent with the well-known inverse relationship between expansion factors and wind speed [e.g., *Wang and Sheeley*, 1997; *Neugebauer et al.*, 1998]. Beyond 3.5 R_{sun}, on the other hand, we know that the width of the coronal hole, as sampled by UVCS (see Figure 4) is similar to that sampled by Ulysses: Hence the flow becomes radial in the first few solar radii.

[62] The lower speed of low-latitude wind, measured by in situ experiments, corresponds to a lower outflow speed at coronal levels. Values for wind speed at 3.5 and 4.5 R_{sun} are given in Figure 9 and Table 2. What is perhaps more interesting is the evidence we found that the acceleration region of the solar wind, at low latitudes, extends over a longer altitude range than it does in polar holes. If we take 3.5 R_{sun} as a reference level, we find a proton outflow speed on the order of one-fifth of the terminal wind speed, in low-latitude regions, with respect to an outflow speed on the order of one-third of the terminal speed in polar holes [*Cranmer et al.*, 1999].

[63] Wind emanating from streamer regions is slower than coronal hole low-latitude wind by ~20%, in terminal speed, over the time we analyzed. At coronal levels, this translates into a factor of 3 difference, in speed, at altitudes 3.5 and 4.5 R_{sun}. Our results imply also a shift to higher distances of the region where plasma gets accelerated: Apparently the slower the outflow speed the higher is the acceleration region. However, because we have only data at two levels, it is hard to say where acceleration occurs, both in low-latitude coronal holes and in streamer regions.

[64] Oxygen ions move faster than protons, in coronal holes and streamer regions, in agreement with previous findings and theoretical predictions [e.g., *Ofman*, 2000; *Cranmer et al.*, 1999]. If we consider the estimate of *Miralles et al.* [2001] as providing a typical OVI ion outflow speed at 3 solar radii and join their data point to ours, it turns out that the region where oxygen ions are accelerated is below the 3.5 R_{sun} level, at least in low-latitude coronal holes.

[65] As to the variability of solar wind, since Ulysses was at ≈5 AU, not much can be said, as we expect smaller fluctuations to be modified by dynamical interactions. However, it is worth pointing out that the separation between coronal hole and streamer flow is unambiguously identifiable in in situ data, even at such large distances. The variability we observe may offer a clue to the phenomena which cause it: Open field regions, interspersed amidst closed coronal loops/streamers, at low latitude, are individually sampled by in situ experiments and are possibly responsible for the high wind variability of the low-latitude wind. It may be difficult to detect the same level of variability at lower coronal level, because, unless observations are made at high altitudes, integration effects level out spatially limited flow speed excursions.

6.2. Electron Temperatures in the Extended Corona

[66] As we said, the knowledge of the electron temperatures in the extended corona is so poor that this is one of the most uncertain parameters of the calculations. Perhaps we have more information on T_e from OVI ions than from protons because SWICS O^{7+}/O^{6+} data (see Figure 8) indicate, in the first half of the campaign, a lower T_e than at later times. On the basis of this constraint, we reproduced the OVI doublet line intensities using electron temperatures of 1.3 10^6 K in coronal hole regions and 1.5 10^6 K in streamers.

[67] The values we adopted are within the range of the SWICS data for plasma originating in the coronal regions we observed and can be compared with previous results from other authors. Oxygen freeze-in temperatures have recently been measured by *Hefti et al.* [2000] using the charge time-of-flight (CTOF) mass and charge spectrometer of CELIAS (Charge Element and Isotope Analysis

Table 3. Oxygen Freezing-In Temperature and Abundance

Structure	Freezing-In Temperature, K	Oxygen Abundance
Coronal Hole	$1.3\ 10^6$	8.55
Streamer	$1.5\ 10^6$	8.73

System) on board of SOHO. These authors confirm the anticorrelation between the freezing-in temperature (T_{76}) derived from the O^{7+}/O^{6+} ratio and the solar wind speed, observed earlier [e.g., *Galvin et al.*, 1984] and give values of T_{76} for the equatorial coronal hole, which on the following rotation would become the target of WSM1 analysis. This data are especially relevant to us, as they come from a situation similar to the one we are analyzing at present. As SOHO crossed the boundary of the coronal hole, *Hefti et al.* [2000] found a sudden increase of T_{76} from $1.3\ 10^6$ K to $1.6\ 10^6$ K. *Hefti et al.* [2000] give uncertainties on the order of 10%: Hence the values of T_e, which allowed us to reproduce the observed OVI line intensities, are in excellent agreement with the latter authors' findings. Our results are also in good agreement with the T_{65} (through the O^{6+}/O^{5+} ratio) versus wind speed profile given by *Grünwaldt et al.* [1999]. Table 3 summarizes freezing-in temperatures and oxygen abundances from our analysis. What quadrature observations allow us to do is to set limits to the altitude, in the corona, where OVI ions are frozen-in. As our observations refer to altitudes $r = 3.5 - 4.5\ R_{\rm sun}$, oxygen ions freeze-in below these levels, both in coronal holes and streamer regions. It is beyond the scope of this paper to make a detailed study of the profile of the oxygen ionization state versus altitude, in the corona, as we should know the radial profiles of electron temperature, density, and OVI ions outflow speed at levels below those analyzed in the present work. Still we can check whether the physical parameters we derived at 3.5 and 4.5 $R_{\rm sun}$ are compatible with OVI ions freezing-in conditions. To this end, we examined both the streamer and coronal hole regions and compared the coronal expansion time with the OVI ionization equilibrium time.

[68] We define the expansion timescale τ_{exp} as the time it takes particles to flow through one density scale height $\tau_{exp} = [(V_{\rm out}/n_e)|dn_e/dr|]^{-1}$. The density scale height has been calculated from the n_e versus r profiles derived from LASCO pB data, and it is rather ill defined at 3.5 $R_{\rm sun}$, as profiles are given only for larger altitudes. Expansion times turn out to be on the order of $\approx 10^4$ s.

[69] The ionization timescale is defined as $\tau_{eq} = 1/[n_e\,(C_i + A_i + R_r + D_r)]$, where C_i and A_i are the collisional ionization and autoionization rates and R_r and D_r are the radiative and dielectronic recombination rates. Independent of the altitude, and both in streamers and coronal hole regions, the collisional ionization rate is the highest, among the processes we considered, and is on the order of $10^{-10}-10^{-11}$ $\rm cm^3\ s^{-1}$ (we refer to *Arnaud and Rothenflug* [1985] for ionization rates, to *Verner and Ferland* [1996] for radiative recombination rates, and to *Mazzotta et al.* [1998] for dielectronic recombination rates). The expansion timescale is much shorter than the OVI ionization timescale in the coronal hole, at 3.5 and 4.5 $R_{\rm sun}$, and, in the streamer, at 4.5 $R_{\rm sun}$. In streamers at 3.5 $R_{\rm sun}$ the expansion timescale is at the same order as, but smaller than, the OVI ionization timescale. This confirms that the freezing-in assumption for O^{5+} is valid. Hence we found that the conclusions we drew that oxygen ions are frozen-in at and beyond 3.5 $R_{\rm sun}$ are consistent with order of magnitude calculations of τ_{exp} and τ_{eq}.

[70] Hydrogen is known to freeze-in at higher altitudes than oxygen, which means we expect, in case, a lower freezing-in temperature for hydrogen than for oxygen. This qualitative result is confirmed by our calculations. *Withbroe et al.* [1982] suggested the lifetime of hydrogen atoms to become shorter than the coronal expansion time for $r \leq 8$ $R_{\rm sun}$ in equatorial regions and for $r \leq 3$ $R_{\rm sun}$ in polar coronal holes. In these regions hydrogen atoms and protons should be coupled. Our results are in agreement with Withbroe's results in coronal holes (we remind the reader that the equatorial hole we analyze has higher densities than polar holes and freezing-in is expected at higher altitudes), but in streamers, at ≈ 4.5 $R_{\rm sun}$, we had to adopt about the same T_e as at lower levels to be able to reproduce the Lyman-α intensity, which might be taken as an indication that hydrogen is frozen-in at that level. Calculations analogous to those outlined above for OVI ions, however, show that hydrogen is still far from freezing-in conditions. The reason for this discrepancy is not clear, but it should most probably be interpreted as hinting to a temperature decrease with altitude much slower than in the streamer region analyzed by *Gibson et al.* [1999].

[71] We would like to conclude the paper by again reminding the reader of the benefits we get from making use of quadrature observations. The low-latitude wind mass flux is highly variable [*McComas et al.*, 2000], and at a latitude of $\approx 15°$ (which is approximately the latitude of Ulysses at the time of the Fall 1998 quadrature) it can easily change by a factor 5. It is a tempting, and often adopted, technique to derive the coronal proton flow speed by assuming mass flux conservation, coronal densities, and an a priori magnetic field geometry. However, this procedure gives correct results only in the steady polar wind. In the highly variable low-latitude wind, the average in situ mass flux value allows one to derive coronal outflow speeds only when uncertainties by a factor of 2–5 are acceptable. At the time of quadratures, however, the precise connection between coronal and in situ plasma limits the risk of such large errors.

[72] **Acknowledgments.** The research of GP has been partially supported by ASI. The research of STS has been supported by the Ulysses/SWOOPS experiment team (D. J. Comas, PI). We thank Ulysses/VHM/FGM (A. Balogh, PI), Ulysses/SWICS (G. Gloeckler and J. Geiss, Co-PIs), SOHO/LASCO (R. Howard, PI), and Sacramento Peak and Wilcox Solar Observatories for use of their data. SOHO and Ulysses are missions of international cooperation between ESA and NASA.

[73] Janet G. Luhmann thanks Robert J. Forsyth and David F. Webb for their assistance in evaluating this paper.

References

Aellig, M. R., S. Hefti, H. Grünwaldt, P. Bochsler, P. Würz, F. M. Ipavich, and D. Hovestadt, The Fe/O elemental abundance as observed with SOHO/CELIAS/CTOF, *J. Geophys. Res.*, *104*, 24,769, 1999.

Arnaud, M., and R. Rothenflug, An updated evaluation of recombination and ionization rates, *Astron. Astrophys. Suppl. Ser.*, *60*, 425, 1985.

Bromage, B. I. J., D. Alexander, A. Breen, J. R. Clegg, G. Del Zanna, C. DeForest, D. Dobrzycka, N. Gopalswamy, B. Thompson, and P. K. Browning, Structure of a large low altitude coronal hole, *Sol. Phys*, *193*, 181, 2000.

Brueckner, G. E., et al., The large angle spectroscopic coronagraph (LASCO), *Sol. Phys.*, *162*, 357, 1995.

Cranmer, S. R., et al., An empirical model of a polar coronal hole at solar minimum, *Astrophys. J.*, *511*, 481, 1999.

Del Zanna, G., and B. I. J. Bromage, The Elephant's Trunk: Spectroscopic diagnostics applied to SOHO/CDS observations of the August 1996 equatorial coronal hole, *J. Geophys. Res.*, *104*, 9753, 1999.

Dobrzycka, D., A. Panasyuk, L. Strachan, and J. L. Kohl, Comparison of polar and equatorial coronal holes observed by UVCS/SOHO: Geometry and physical properties, *Space Sci. Rev.*, *87*, 173, 1999.

Domingo, V., B. Fleck, and A. I. Poland, The SOHO mission: An overview, *Sol. Phys.*, *162*, 1, 1995.

Fineschi, S., L. D. Gardner, J. L. Kohl, M. Romoli, and G. Noci, Grating stray light analysis and control in the UVCS/SOHO, *Proc. SPIE Int. Soc. Opt. Eng.*, *3443*, 67, 1998.

Forsyth, R. J., and J. T. Gosling, Corotating and transient structures in the heliosphere, in *The Heliosphere Near Solar Minimum: The Ulysses Perspective*, edited by A. Balogh, R. G. Marsden, and E. J. Smith, p. 107, Springer, New York, 2001.

Galvin, A. B., F. M. Ipavich, G. Gloeckler, D. Hovestadt, B. Klecker, and M. Scholer, Solar wind ionization temperatures inferred from the charge state composition of diffuse particle events, *J. Geophys. Res.*, *89*, 2655, 1984.

Galvin, A. B., Minor ion composition in CME-related solar wind, in *Coronal Mass Ejections*, *Geophys. Monogr. Ser.*, vol. 99, edited by N. Crooker, J. A. Joselyn, and J. Feynman, p. 253, AGU, Washington, D.C., 1997.

Galvin, A. B., and J. L. Kohl, Whole Sun Month at solar minimum: An introduction, *J. Geophys. Res.*, *104*, 9673, 1999.

Gardner, L. D., et al., Stray light, radiometric, and spectral characteristics of UVCS/SOHO: Laboratory calibration and flight performances, *Proc. SPIE Int. Soc. Opt. Eng.*, *2831*, 2, 1996.

Geiss, J., et al., The southern high-speed stream: Results from the SWICS instrument on Ulysses, *Science*, *268*, 1033, 1995.

Gibson, S. E., A. Fludra, F. Bagenal, D. Biesecker, G. Del Zanna, and B. I. J. Bromage, Solar minimum streamer densities and temperatures using Whole Sun Month coordinated data sets, *J. Geophys. Res.*, *104*, 9691, 1999.

Gloeckler, G., J. Geiss, H. Balsiger, P. Bedini, J. C. Cain, J. Fisher, L. A. Fisk, A. B. Galvin, F. Gliem, and D. C. Hamilton, The solar wind ion composition spectrometer, *Astron. Astrophys. Suppl. Ser.*, *92*, 267, 1992.

Gosling, J. T., G. Borrini, J. R. Asbridge, S. J. Bame, W. C. Feldman, and R. T. Hansen, Coronal streamers in the solar wind at 1 AU, *J. Geophys. Res.*, *86*, 5438, 1981.

Gosling, J. T., and V. J. Pizzo, Formation and evolution of corotating interaction regions and their three dimensional structure, *Space Sci. Rev.*, *89*, 21, 1999.

Grünwaldt, H., M. Hilchenbach, M. R. Aellig, F. M. Ipavich, K.-U. Reiche, D. Hovestadt, and B. Wilken, O^{5+} observations from various solar wind speeds, in *Solar Wind IX: Proceedings of the Ninth International Solar Wind Conference*, edited by S. R. Habbal et al., p. 259, Am. Inst. of Phys., Woodbury, N. Y., 1999.

Habbal, S. R., R. Esser, M. Guhathakurta, and R. Fisher, Flow properties of the solar wind derived from a two-fluid model with constraints from white light and in situ interplanetary observations, *J. Geophys. Res. Lett.*, *22*, 1465, 1995.

Habbal, S. R., R. Woo, S. Fineschi, R. O'Neal, J. L. Kohl, G. Noci, and C. Korendyke, Origins of the slow and ubiquitous fast solar wind, *Astrophys. J.*, *489*, L103, 1997.

Hefti, S., H. Grünwaldt, P. Bochsler, and M. R. Aellig, Oxygen freeze-in temperatures measured with SOHO/CELIAS/CTOF, *J. Geophys. Res.*, *105*, 10,527, 2000.

Hyder, C. L., and B. W. Lites, H_α; Doppler brightening and Lyman$_\alpha$; Doppler dimming in moving H$_\alpha$; Prominences, *Sol. Phys.*, *14*, 147, 1970.

Ko, Y.-K., L. A. Fisk, J. Geiss, G. Gloeckler, and M. Guhathakurta, An empirical study of the electron temperature and heavy ion velocities in the South polar coronal hole, *Sol. Phys.*, *171*, 345, 1997.

Kohl, J. L., et al., First results from the SOHO Ultraviolet Coronograph Spectrometer, *Sol. Phys.*, *175*, 613, 1997.

Kopp, R. A., and T. E. Holzer, Dynamics of coronal hole regions: Steady polytropic flows with multiple critical points, *Sol. Phys.*, *49*, 43, 1976.

Li, X., S. R. Habbal, J. L. Kohl, and G. Noci, The effect of temperature anisotropy on observations of Doppler dimming and pumping in the inner corona, *Astrophys. J.*, *501*, L133, 1998.

Linker, J. A., et al., Magnetohydrodynamic modeling of the solar corona during Whole Sun Month, *J. Geophys. Res.*, *104*, 9809, 1999.

Mazzotta, P., G. Mazzitelli, S. Colafrancesco, and N. Vittorio, Ionization balance for optically thin plasmas: Rate coefficients for all atoms and ions of the elements H to NI, *Astron. Astrophys. Suppl. Ser.*, *133*, 403, 1998.

McComas, D. J., P. Riley, J. T. Gosling, A. Balogh, and R. Forsyth, Ulysses' rapid crossing of the polar coronal hole boundary, *J. Geophys. Res.*, *103*, 1955, 1998.

McComas, D. J., B. L. Barraclough, H. O. Funsten, J. T. Gosling, E. Santiago-Munoz, R. M. Skoug, B. E. Goldstein, M. Neugebauer, P. Riley, and A. Balogh, Solar wind observations over Ulysses' first full polar orbit, *J. Geophys. Res*, *105*, 10,419, 2000.

Miralles, M. P., S. R. Cranmer, A. V. Panasyuk, M. Romoli, and J. L. Kohl, Comparison of empirical models for polar and equatorial coronal holes, *Astrophys. J.*, *549*, L257, 2001.

Munro, R. H., and B. V. Jackson, Physical properties of a polar coronal hole from 2 to 5 R_s, *J. Geophys. Res.*, *213*, 874, 1977.

Neugebauer, M., et al., The spatial structure of the solar wind and comparisons with solar data and models, *J. Geophys. Res.*, *103*, 14,578, 1998.

Noci, G., J. L. Kohl, and G. L. Withbroe, Solar wind diagnostics from Doppler-enhanced scattering, *Astrophys. J.*, *315*, 706, 1987.

Ofman, L., Source regions of the slow solar wind in coronal streamers, *Geophys. Res. Lett.*, *27*, 2885, 2000.

Pizzo, V. J., Global, quasi-steady dynamics of the distant solar wind, 1, Origin of north-south flows in the outer heliosphere, *J. Geophys. Res.*, *99*, 4173, 1994.

Schühle, U., K. Wilhelm, J. Hollandt, P. Lemaire, and A. Pauluhn, Radiance variation of the quiet Sun at far-ultraviolet wavelengths, *Astron. Astrophys.*, *354*, L71, 2000.

Sheeley, N. R., et al., Measurements of flow speed in the corona between 2 and 30 R_{sun}, *Astrophys. J.*, *484*, 427, 1997.

von Steiger, R., R. Wimmer Schweingrüber, J. Geiss, and G. Gloeckler, Abundance variations in the solar wind, *Adv. Space Res.*, *15*(7), 3, 1995.

Suess, S. T., S. Parhi, and R. L. Moore, The paradox of filamented coronal hole flow but uniform high speed wind, *Eos Trans. AGU*, *79*, 271, 1998.

Suess, S. T., G. Poletto, M. Romoli, M. Neugebauer, B. E. Goldstein, and G. Simnett, May 1997 SOHO-Ulysses quadrature, *J. Geophys Res.*, *105*, 25,033, 2000.

Thieme, K. M., R. Schwenn, and E. Marsch, Are structures in high-speed streams signatures of coronal fine structures?, *Adv. Space Res.*, *9*, 127, 1989.

Thieme, K. M., R. Schwenn, and E. Marsch, Spatial structures in high-speed streams as signatures of fine structures in coronal holes, *Ann. Geophys.*, *8*, 713, 1990.

Verner, D. A., and G. J. Ferland, Atomic data for Astrophysics, I, Radiative recombination rates for H-like, He-like, Li-like, and Na-like ions over a broad range of temperature, *Astrophys. J. Suppl. Ser.*, *103*, 467, 1996.

Wang, Y.-M., and N. R. Sheeley Jr., Solar wind stream interactions and the wind speed-expansion relationship, *Astrophys. J.*, *488*, L51, 1997.

Wenzel, K. P., R. G. Marsden, D. E. Page, and E. J. Smith, The Ulysses Mission, *Astron. Astrophys. Suppl. Ser.*, *92*, 207, 1992.

Withbroe, G. L., J. K. Kohl, and H. Weiser, Probing the solar wind acceleration region using spectroscopic techniques, *Space Sci. Rev.*, *33*, 17, 1982.

Woo, R., S. R. Habbal, R. A. Howard, and C. M. Korendyke, Extension of polar coronal hole boundary into interplanetary space, *Astrophys. J.*, *513*, 961, 1999.

D. Biesecker, L-3 Communications Analytics Corporation, NASA Goddard Space Flight Center, Greenbelt, MD 20771, USA. (doug@sungrazer.nascom.nasa.gov)

R. Esser and Y.-K. Ko, Harvard-Smithsonian Center for Astrophysics, 60 Garden Street, Cambridge, MA 02138, USA. (resser@cfa.harvard.edu; kuen@uvcs14.nascom.nasa.gov)

G. Gloeckler, Department of Physics, University of Maryland, College Park, MD 20742-2425, USA. (gloeckler@umdsp.umd.edu)

G. Poletto, Osservatorio Astrofisico di Arcetri, Largo Enrico Fermi, 5, 50125 Firenze, Italy. (poletto@arcetri.astro.it)

S. T. Suess, NASA Marshall Space Flight Center/SD50, Huntsville, AL 35812, USA. (steve.suess@msfc.nasa.gov)

T. H. Zurbuchen, Department of Atmospheric, Oceanic and Space Sciences, University of Michigan, Ann Arbor, MI 48109, USA. (thomasz@umich.edu)